water

MDPI

Article

Characteristics and Hazards Prevention of Bed Separation Water Inrush: A Case Study of the Cuimu Coal Mine, China

Hewen Ma [1,2,3,4]

[1] CCTEG Xi'an Research Institute (Group) Co., Ltd., Xi'an 710077, China; mahewen@cctegxian.com; Tel.: +86-159-3481-2629
[2] State Key Laboratory of Coal Mine Disaster Prevention and Control, Xi'an 710077, China
[3] Huaibei Mining Group Co., Ltd., Huaibei 235000, China
[4] School of Resources and Geosciences, China University of Mining and Technology, Xuzhou 221008, China

Abstract

This paper presents an active prevention and control technology for bed separation water inrush hazards, the effectiveness of which has been validated. Based on the hazard degree identification of such hazards and corresponding preventive measures, the Fuzzy Analytic Hierarchy Process (FAHP) and Expert Grading System (EGS) are adopted to analyze the prevention mechanisms and determine the indicator weights of different influencing factors. The results show that enhancing drainage capacity and accurately predicting bed separation water inflow are two effective measures to prevent water inrush or reduce the hazard risk coefficient. In addition, controlling the development of water-conducting fractured zones and optimizing drainage measures are also effective approaches to reducing the risk coefficient. The research results provide a theoretical basis and practical guidance for the prevention and control of bed separation water inrush hazards, and offer an effective and cost-efficient method for addressing such mining-induced hazards.

Keywords: bed separation; water-filled bed separation; characteristics of bed separation water inrush; hazards; numerical simulation

1. Introduction

China is abundant in coal resources and ranks as the world's largest coal-producing country. Over 95% of coal resources in China are mined underground, with an average mining depth exceeding 400 m [1–5]. Meanwhile, China is one of the countries suffering the most serious mine water hazards in the world. Among the five major coal mine hazards, coal mine water inrush ranks second only to gas outbursts. The frequent and severe coal mine water inrushes have caused significant economic and property losses to the nation and its people, and also posed great challenges to coal mine safety [6–8]. The safety production situation remains extremely serious.

As a new type of secondary roof water hazard (Figure 1), bed separation water hazard usually presents no obvious precursors before its occurrence. Moreover, the instantaneous water inflow at the panel is extremely large when bed separation water inrush occurs, making such hazards difficult to accurately predict. Therefore, bed separation water hazard is one of the most threatening types of coal seam roof water hazards to coal mine safety [9–12]. Among water inrush accidents in China's coal mines, 27 coal mines have been confirmed to have experienced bed separation water hazards, and these mines are distributed across mining areas in both eastern and western China.

Check for updates

Academic Editor: Pedro Proença Cunha

Received: 28 February 2026
Revised: 23 March 2026
Accepted: 24 March 2026
Published: 28 March 2026

Copyright: © 2026 by the author. Licensee MDPI, Basel, Switzerland. This article is an open access article distributed under the terms and conditions of the Creative Commons Attribution (CC BY) license.

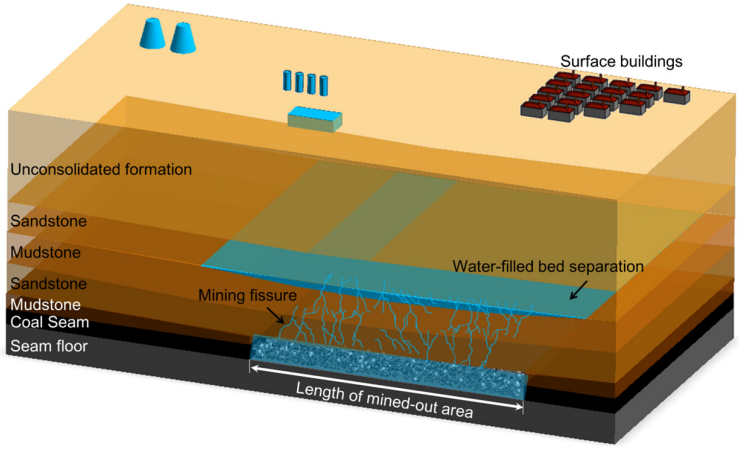


Figure 1. Formation mechanism of bed separation water inrush hazards.

Bed separation water inrush hazards are influenced by multiple factors. Mining induces the formation of water-filled bed separations within the overburden. Shear failure of the underlying strata leads to sudden water inrush into the panel. Analysis of the water-filling conditions of bed separations indicates that shallow bed separations generally lack the necessary conditions for effective water retention. The direct cause of bed separation water inrush is the presence of ultra-thick hard strata in the coal seam roof, whose sudden elastic deformation and fracturing release significant mechanical energy under mining disturbance [13–15]. In addition, water sources and water-conducting channels for bed separation also indirectly contribute to the occurrence of such hazards [16–20]. Some scholars further suggest that underground coal mining causes elastic energy to accumulate in the overlying hard strata; once instability occurs, this energy is instantaneously released, generating transient ultra-high pore pressure in overlying aquifers and thereby triggering mechanical water inrush. In practical cases, these hazards often exhibit periodic initiation and closure of fractures in the water-resisting layer beneath the bed separation with mining disturbance. This is the direct reason for the periodic occurrence of such hazards.

The traditional criterion for identifying the location of bed separation is to compare the lithology of different strata in the overburden and calculate the vertical deformation of the overburden based on the voussoir beam theory, so as to predict the distribution of water-filled bed separation [21–23]. Surface dewatering boreholes, underground diversion boreholes, and barrier boreholes are commonly employed to discharge accumulated water from the panel, proving effective in mitigating bed separation water hazards [13,14,24]. The relationship between coal seam mining distance and water accumulation in bed separations can be used to predict the water volume of bed separations, which can effectively guide practical water detection and drainage engineering and enable the controlled release of bed separation water. However, the overburden above the coal seam roof is a three-dimensional geological body with a massive or stratified structure [25–27]. There is a lack of quantitative prediction for water-filled bed separation at different developmental stages, and there has been no systematic research on proactive prevention and control of bed separation water hazards prior to coal mining. Conducting such research is of great significance for engineering practice.

This research aims to analyze the characteristics and prediction methods of bed separation water inrush. A three-dimensional mechanical model is established to estimate the dimensions of bed separations at different developmental stages. Subsequently, numerical simulations and field measurements are conducted to investigate the characteristics of bed separation water inrush, and analyze the influencing factors and mechanisms of such water hazards. On this basis, the weights of key indicators and a risk assessment model

for bed separation water hazards are proposed. It aims to provide a scientific basis for the prevention and control of bed separation water inrush.

2. Hydrogeological and Engineering Geological Conditions

The Cuimu Coal Mine is located in Baoji City, Shaanxi Province, China (Figure 2). It covers approximately 37.5 km^2 and has a designed capacity of 4.0 million tons per year. It is situated on the southern edge of the Longdong Loess Plateau and at the eastern end of the Yonglong Mining Area. From top to bottom, the aquifers in this mine include the Quaternary pore-fissure phreatic aquifer, Cretaceous Luohe Formation and Yijun Formation confined aquifers, Jurassic Zhiluo Formation and Yan'an Formation aquifers, and Triassic Tongchuan Formation aquifer. The Cretaceous Luohe Formation sandstone aquifer is the major one. Overall, the aquifers have a specific discharge ranging from 0.00948 to 0.08946 L/s●m and a permeability coefficient of 0.002446 to 0.03354 m/d, indicating weakly water-rich aquifers.

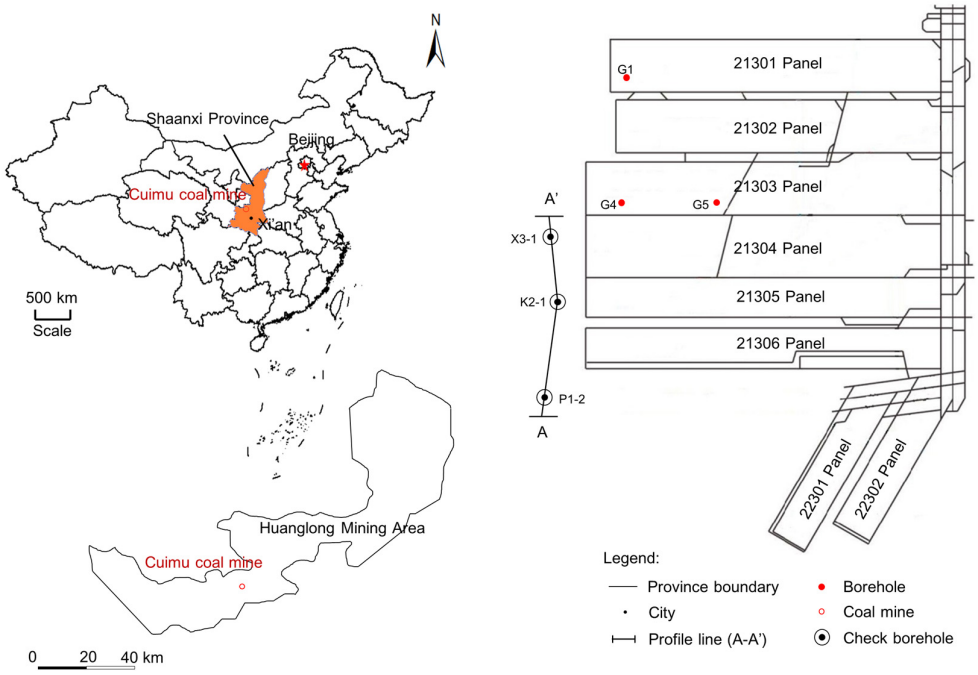


Figure 2. Location of the Cuimu Coal Mine.

There are no major water-controlling structures along the boundary of the Cuimu Coal Mine. The coal-bearing strata generally have a gentle dip angle, typically ranging from 3° to 5°, with a maximum of 17°. No water inrush hazards caused by faults have been observed during roadway excavation. The Yan'an Formation is the coal-bearing stratum in this area, in which the No. 3 coal seam is the primary mining seam and is classified as a relatively stable seam. The burial depth of the No. 3 coal seam ranges from a minimum of 314.42 m to a maximum of 777.03 m, with most areas between 400 and 500 m. The roof of the No. 3 coal seam is predominantly composed of dark-gray mudstone, sandy mudstone, siltstone, and fine- to medium-grained sandstone, with a maximum thickness of 12.76 m. The floor consists of gray to dark-gray mudstone, gray-brown aluminous mudstone, or aluminous siltstone to fine-grained sandstone, with a thickness ranging from 0.20 m to 18.30 m. The rocks at the roof and floor of the No. 3 coal seam have different strengths [28,29]; sandstone, siltstone and mudstone belong to hard, medium-hard and soft rock according to the Code for Investigation of Geotechnical Engineering (MOHURD 2002), respectively.

Based on the engineering geological properties and genetic types of the overburden at Cuimu Coal Mine, the overlying strata can be divided into four soil layers and four lithological types (Table 1), as illustrated in the geological profile (Figure 3). Mining is primarily conducted in the Jurassic Yan'an Formation coal seams, with the Cretaceous Luohe Formation serving as the principal aquifer. The lithology of the strata between the coal seams and the Luohe Formation mainly consists of mudstone, sandstone, and conglomerate. The Luohe Formation is characterized by an extremely large thickness, exceeding 100 m and reaching a maximum of 550 m, and its water abundance varies considerably. Similarly, the coal seams are exceptionally thick, generally over 10 m and ranging from 20 to 30 m at their maximum.

Table 1. Engineering geological types of overburden in the Cuimu Coal Mine.

Type	Rock Group	Spatial Distribution	Structural Characteristics
Soil groups	Quick sand-silt stratum group	Distributed as strips and bands in the river floodplain	Dispersed structure
	Sand-gravel stratum group	Distributed in the form of strips and bands in the riverbed sections	—
	Loess stratum group	Distributed in residual hills, beam-like hills and hilltop sections	—
	Clay stratum group	Distributed in gully heads and watershed sections	—
Rock Types	Conglomerate	Dominated by the Yijun Formation, followed by the Luohe Formation	Massive blocky structure
	Sandstone	Dominated by the Luohe Formation, followed by the Zhiluo, Yan'an and Anding Formations	Layered structure
	Mudstone	Dominated by the Anding Formation, followed by the Yan'an and Zhiluo Formations	Thin-layered structure
	Coal	Dominated by the lower coal seam, followed by the middle and upper coal seams	Massive blocky structure

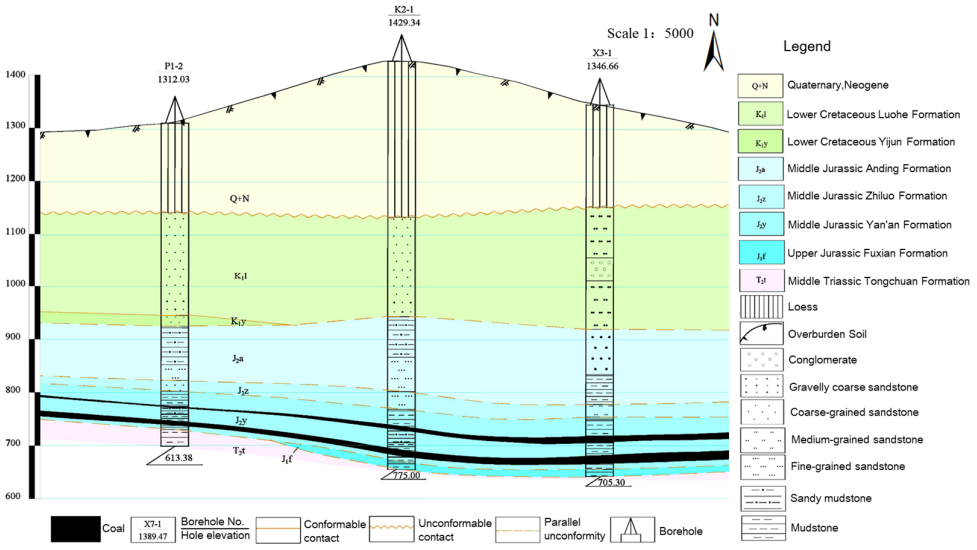


Figure 3. A-A' geological cross section of the Cuimu Coal Mine.

3. Method

3.1. Prediction of Water-Accumulated Bed Separation

Clayey and argillaceous cemented materials in rock strata or weak structural planes between rock strata can interact with water molecules and undergo softening, leading to softening deformation and expansion of the rock strata, thereby reducing the bearing capacity of the overburden. Transverse fissure water in the rock mass exerts hydrostatic pressure perpendicular to the rock plates. Under tensile stress, the deflection of transverse fissures within the strata gradually increases, thereby altering the internal structure of the rock strata.

During coal seam excavation, the overlying strata are subjected only to the load of the upper rock mass, and then bed separation between rock strata develops and bed separation fractures are generated inside the overburden. When the water-filled conditions for bed separation are satisfied within the overburden, the internal cavity of the bed separation is gradually filled with water, forming a water-filled bed separation bag. At this time, the rock strata at the bottom of the bed separation are under the combined action of the overlying rock mass and hydrostatic pressure from the water-filled bed separation bag. Variations in overburden load lead to differential bending of the strata adjacent to the bed separation, causing uneven vertical displacement in the overlying rock mass.

Because the bottom rock strata of the bed separation experience non-uniform distributed loads, nonlinear deflections arise during shear deformation, which leads to the nonlinear growth of the bed separation. In the mechanical model of water-filled bed separation, the volumetric strain of the bed separation is defined as the difference between the volumetric strain induced by the overburden load and the volumetric strain under hydrostatic pressure.

Assuming bed separation develops between the $(n-1)$-th and n-th strata (Figure 4), the vertical displacement of the initial bed separation under four-edge clamped boundary conditions is given by $\omega = \omega_{n-1} - \omega_n$. Assuming the thickness of the thin plate is h, its lengths in the x and y directions are a and b, respectively (Figure 5). The plate is subjected to a uniformly distributed load q_o in the direction perpendicular to the plate surface. When the bed separation becomes water-filled, the bottom of the water-filled bed separation bends downward under hydrostatic pressure (q). The vertical displacement of the bed separation is the difference between the bending deflection of the strata under hydrostatic pressure and that under overburden load. This difference represents the increase in the vertical gap of the initial bed separation under the four-edge clamped boundary conditions, which is given below:

$$\Delta\omega_1 = \frac{q_o}{16\pi^4 D\left(\frac{3}{a^4} + \frac{3}{b^4} + \frac{2}{a^2b^2}\right)}\left(1 - \cos\frac{2m\pi x}{a}\right)\left(1 - \cos\frac{2n\pi y}{b}\right), \tag{1}$$

Assuming bed separation develops between the $(n-1)$-th and n-th strata, the increase in the vertical gap of the periodically developing bed separation under the three-edge clamped and one-edge simply supported boundary conditions is given below:

$$\Delta\omega_2 = \frac{q_o x\left(\frac{5}{2} - \frac{3}{2\pi^2} - 3a\right)}{\pi^2 D\left(\frac{24}{a^3} - \frac{12}{a^2} + \frac{8\pi^2}{a} + \frac{3}{a}\right)}\left(1 - \cos\frac{2\pi x}{a}\right)\left(1 - \cos\frac{2\pi y}{b}\right), \tag{2}$$

where the $\Delta\omega_1$ is the increment of the vertical gap in the initial bed separation under four-edge clamped boundary conditions, $\Delta\omega_2$ is the increase in the vertical gap of the periodically developing bed separation under the three-edge clamped and one-edge simply supported boundary conditions, a and b represent the strike advance distance and the

dip width of the mined panel, respectively. The rectangular thin plate is subjected to a uniformly distributed load $q_o = \gamma H$ from the overburden strata, where γ is the unit weight of the rock strata and H is the thickness of the strata.

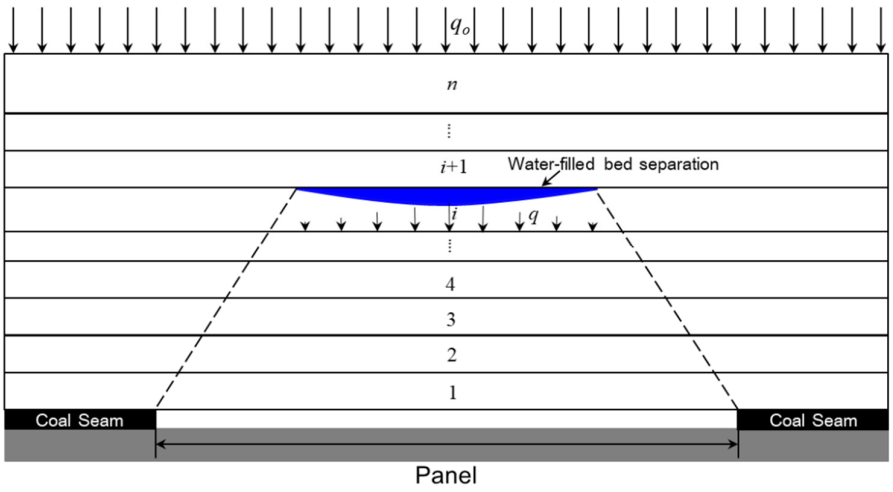


Figure 4. Mechanical model of bed separation space in overburden.

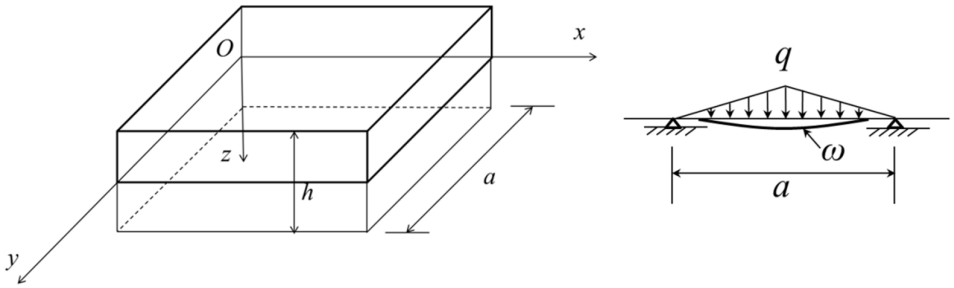


Figure 5. Mechanical model of bed separation development under distributed load and hydrostatic pressure.

The volume of bed separation formed within the overburden strata is the integral of the vertical displacement caused by internal rock deformation. Therefore, substituting Equations (1) and (2) into Equation (3) under hydrostatic pressure gives the expanded volume of the initially developing bed separation and the periodically developing bed separation.

$$V_e = \iint_D D\nabla^4 \omega dxdy, \tag{3}$$

3.2. Numerical Simulation

The fluid–solid coupling in FLAC^{3D} 3.0, a finite difference code, is used to analyze the development of bed separation under hydrostatic pressure, focusing on the effect of water accumulation inside the bed separation on the deflection of the strata at the base of the bed separation. The application of hydrostatic pressure in a certain region inside the overburden is adopted to simulate the formation of a water-filled bed separation in the overburden. Under mining-induced influence, the dynamic evolution of overburden deformation above the coal seam is simulated during panel advancement under the hydrostatic pressure of water accumulation in the bed separation. The dynamic response results of the overburden

rock mass are obtained. An ideal elastoplastic constitutive model using the Mohr–Coulomb yield criterion is adopted in this study to characterize the strength behavior of rock mass.

$$f_s = \sigma_1 - \sigma_3 \frac{1+\sin\varphi}{1-\sin\varphi} - 2c\sqrt{\frac{1+\sin\varphi}{1-\sin\varphi}}, \quad (4)$$

where f_s is the rock mass strength, σ_1 and σ_3 are the major and minor principal stresses, respectively, and c and φ denote the cohesion and friction angle. Shear failure occurs in the rock mass when $f_s > 0$. Tensile failure is additionally assessed based on the tensile strength criterion: $\sigma_3 \leq \sigma_T$ (with tensile stress taken as positive, σ_T is the uniaxial tensile strength).

Figure 6 shows the schematic diagram. According to the engineering geological and mining conditions of the 21303 panel where bed separation water inrush occurred in the study area, the simulation model dimensions are set at 760 m × 400 m × 562.6 m (length × width × height). The coal seam mining height is 10.6 m, and the dip width and strike length of the panel are 200 m and 560 m, respectively. A 100-m coal pillar is reserved around the panel to reduce the boundary effect. Table 2 presents the mechanical properties of the overburden obtained through laboratory experiments. Meanwhile, the model has a free top boundary, while its bottom and horizontal boundaries are fixed.

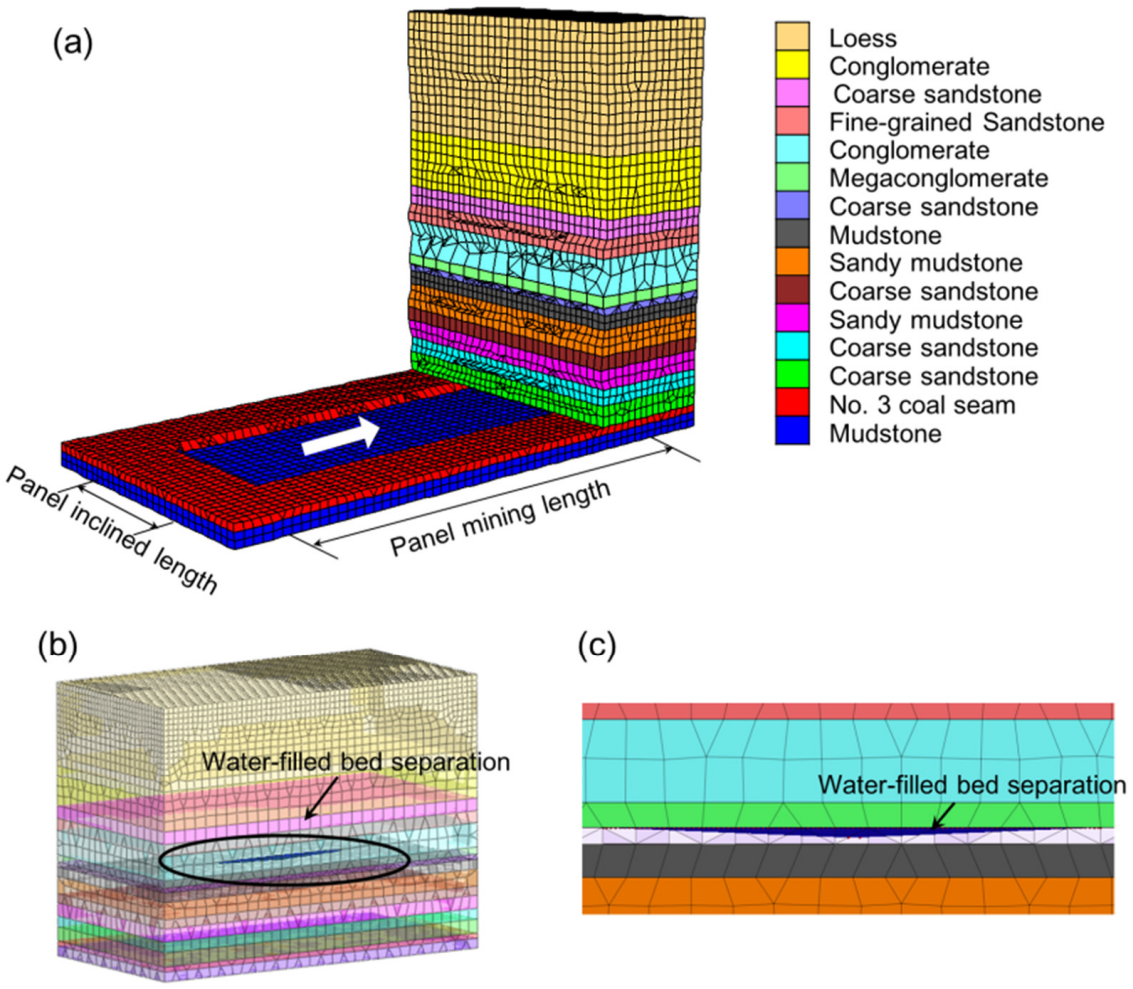


Figure 6. Numerical simulation model: (**a**) structure diagram, (**b**) perspective view, (**c**) partial enlarged view.

Table 2. Physico-mechanical parameters of rocks.

Stratum Lithology	Thickness (m)	Elastic Modulus (MPa)	Tensile Strength (MPa)	Shear Modulus (GPa)	Density (g/cm^3)	Poisson's Ratio	Internal Friction Angle (°)
Loess	172.05	280	0.13	0.776	1.45	0.32	20.00
Conglomerate	81.08	30,240	1.68	3.120	2.48	0.15	39.12
Coarse sandstone	26.16	4580	0.24	2.450	2.24	0.24	35.62
Fine sandstone	24.50	7540	0.42	1.820	2.31	0.23	36.42
Conglomerate	49.41	25,140	1.35	2.610	2.54	0.19	38.54
Megaconglomerate	14.97	27,540	1.52	2.950	2.48	0.23	38.24
Coarse sandstone	10.27	3250	0.24	2.420	2.20	0.25	35.85
Mudstone	20.60	4680	0.12	1.340	2.41	0.23	35.12
Sandy mudstone	33.85	5520	0.12	1.460	2.38	0.22	36.46
Coarse sandstone	18.95	4010	0.24	2.430	2.21	0.23	36.42
Sandy mudstone	26.98	15,240	0.88	1.620	2.33	0.20	38.65
Coarse sandstone	22.20	11,250	0.65	1.230	2.25	0.19	37.86
Coarse sandstone	29.36	7580	0.65	1.850	2.35	0.18	38.12
No. 3 coal seam	10.60	5240	0.24	0.540	1.35	0.18	37.54
Mudstone	20.00	10,080	0.58	1.100	2.34	0.22	36.42

3.3. Field Measurements

Since the operation of the Cuimu Coal Mine, a total of 26 bed separation water inrush hazards have occurred in the No. 21303 panel, which seriously affected the safe production of the coal mine. During the excavation period of the panel, there was a clear connection between the water level changes and the evolution process of bed separation water inrush. The precise identification of mine water inrush sources offers a scientific basis for the formulation of mine water hazard prevention and control strategies. In this study, monitoring of water inflow in the panel and detection of water-rich anomalies in the overburden above the coal seam roof can identify the source of the water inrush. The water inflow of the panel is correlated with the mining distance and coal seam mining height, thereby providing an accurate reference for the prevention and control of bed separation water inrush hazards.

4. Results and Analysis

4.1. Excavation Mechanism of Bed Separation Development

The rock mass undisturbed by mining is constrained by surrounding boundary conditions and maintains a state of natural stress equilibrium. The internal stress of rock masses at different horizons is mainly affected by the overburden load and lithology. After coal extraction, under the combined action of self-weight stress and overburden load, the stress in the overburden gradually changes from compressive stress to tensile stress, leading to downward bending, fracturing and caving of the coal seam roof, with horizontal fractures developing normal to the joint surfaces. During the advancement of the panel, under the combined effects of shear failure and interlayer separation at contact surfaces, the overlying strata undergo downward bending deformation. Meanwhile, rock masses at different horizons undergo lateral displacement along bedding planes, resulting in shear failure and further separation between strata of different lithology. When strata movement reaches the maximum subsidence displacement, the bed separation becomes fully developed and reaches its maximum internal size. The location and height of bed separation development

migrate with the advancement of the panel, and the greater the coal seam mining thickness, the larger the developed bed separation will be.

Coal seams with shallow burial depth may result in the caving zone or water-conducting fractured zone in the overburden being directly exposed to the ground surface. Under such circumstances, the overburden lacks the conditions for the development of bed separation. Under the same coal seam depth, the inclined length of the panel directly determines the equilibrium structure within the overburden. The maximum mining dimension when the panel reaches the limit arch corresponds to the optimal mining size associated with the maximum bed separation space. Under the same mining conditions, the development duration of bed separation is negatively correlated with the advancing speed of the panel.

Data on coal seam mining height and the measured fracturing-to-mining ratio (FMR) from multiple mines in the Huanglong Coalfield were used to establish their relationship. As shown in Figure 7, when the mining height is less than 8 m, FMR exhibits a significant nonlinear decreasing trend with increasing mining height. When mining height exceeds approximately 8 m, FMR tends to stabilize. At a mining height of about 11.27 m, FMR shows a slight nonlinear trend of decreasing first and then increasing, remaining stable within the range of 21.6–24.2. Based on an analysis of the engineering geological profile of the Cuimu Coal Mine (Figure 3), the water-conducting fractured zone can extend into the bed separation and the fractured aquifer in the glutenite of the Yijun Formation or the Luohe Formation under mining disturbance.

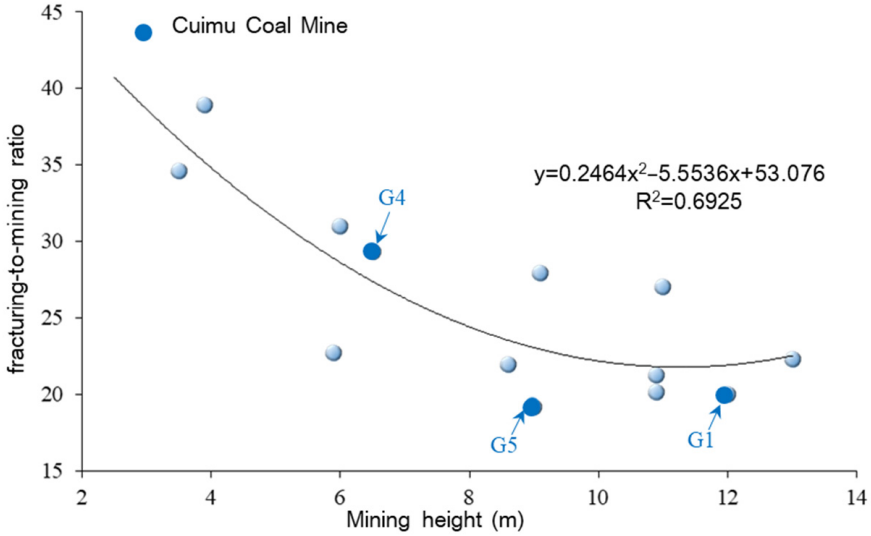


Figure 7. Ratio of fractured zone height to mining height.

4.2. Dynamic Hazard Mechanism of Water-Filled Bed Separation

Different water accumulation volumes in the bed separation lead to varying loads on the underlying strata (Figure 8). The maximum principal stress is symmetrically distributed along the centerline of the goaf. When a water-filled bed separation develops in the overburden, an obvious stress anomaly zone appears in the rock mass nearby. Moreover, as the water volume within the bed separation increases, the area of stress anomaly zones in the overburden expands accordingly. Tensile stress occurs near the water-filled bed separation, and its magnitude is positively correlated with the water filling ratio (pore pressure).

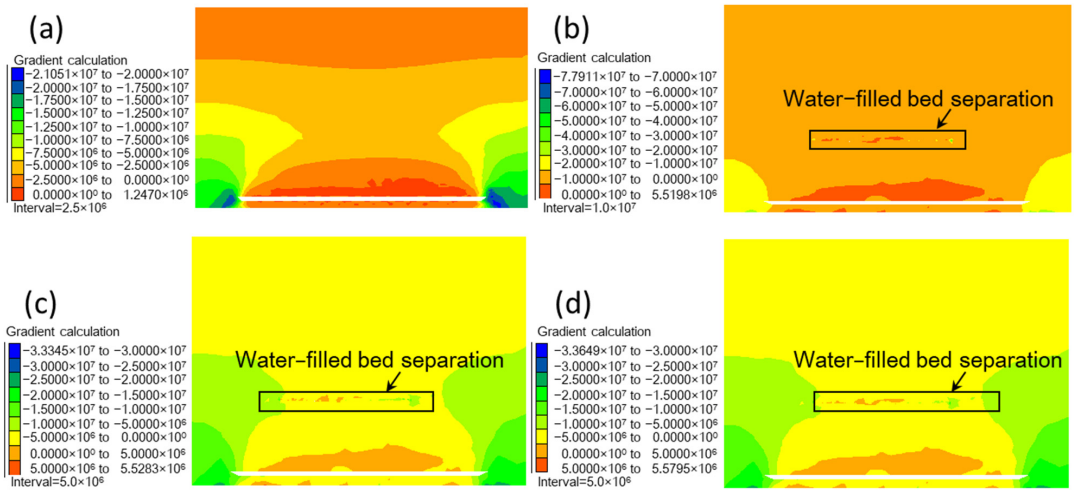


Figure 8. Vertical stress contours in bed separation under varying water filling ratios: (**a**) no water, (**b**) 0.5%, (**c**) 1.5%, and (**d**) 2.5%.

When the bed separation is not filled with water (no pore pressure), the underlying strata of the bed separation are subjected to a compressive stress of 2.5–5 MPa. With the advancement of the panel, water from the overlying aquifer begins to flow into the bed separation, and an obvious stress anomaly zone appears at the water-filled bed separation. The rock mass near the water-filled bed separation is subjected to a compressive stress of 5–10 MPa. At a water filling ratio of 0.5%, the water-filled bed separation is locally subjected to a maximum tensile stress of 5.52 MPa; at 1.5%, the maximum tensile stress is 5.53 MPa; and at 2.5%, it increases to 5.58 MPa.

Figure 9 shows that the vertical deformation of the overburden above the goaf increases with the water volume in the bed separation. This indicates that water-filled bed separation enhances the degree and extent of overburden failure induced by coal mining. This effect is attributed to the elevation of pore pressure, which reduces the effective stress and weakens the mechanical integrity of the strata, thereby promoting tensile and shear failure propagation. When the water filling ratios of the bed separation are 0%, 0.5%, 1.5%, and 2.5%, the maximum vertical displacement above the panel is 5.1687 m, 5.3365 m, 5.3416 m, and 5.3421 m, respectively. The maximum vertical displacement is positively correlated with the water filling ratio.

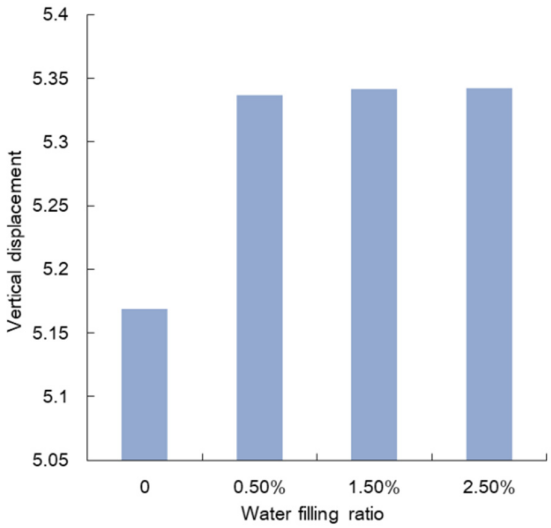


Figure 9. Vertical displacement of underlying strata in water-filled bed separation.

As pore pressure acts on the bed separation as water flows into it, the deformation of the overburden under mining disturbance increases significantly (Figure 9). Furthermore, with an increase in water volume within the bed separation, the subsidence shows a positive increasing trend with the water filling ratio (pore pressure).

4.3. Characteristics and Hazard Prevention of Bed Separation Water Inrush

4.3.1. Characteristics of Bed Separation Water Inrush

Frequent water inrush events occurred at the 21303 panel over a short period, with a total of 14 events. Of these, 4 events were mainly attributed to the release of static reserves from the overlying aquifers, while 10 events were dominated by water inrush from the bed separation and re-inflow due to water recharge into pre-formed bed separation. The water inflow rate was relatively high at the peak of water inrush, reaching a maximum of 570 m^3/h. In addition, the mining distances of the panel corresponding to multiple short-term large water inflow events were similar. The abnormal water inflow of the panel was correlated with the low-resistivity anomaly areas detected by geophysical prospecting. When abnormal water inflow occurred at the 21303 panel, the water level of the Luohe Formation also changed correspondingly.

Based on water inflow monitoring and detection of water-bearing anomaly zones in the coal seam roof, the water level of the Luohe Formation aquifer began to decline after abnormal water inrush occurred at the 21303 panel in Cuimu Coal Mine. When the panel was advanced to 276 m, 313 m, and 430 m, water-rich anomalies existed in the overburden, attributed to the release of static reserves from the overlying aquifers. When the panel was advanced to 567 m, 576 m, 580 m, and 597 m, the water level of the Luohe Formation showed a corresponding downward trend after abnormal water inrush occurred. Specifically, the abnormal water inrush at 567 m was caused by the combined effect of static reserve release from the aquifer and water inrush from the bed separation, while the abnormal water inrush events at 576 m, 580 m, and 597 m were attributed to re-inflow due to water recharge into pre-formed bed separation. Multiple abnormal water inrush events after July 14 were analyzed to be dominated by bed separation water inrush and re-inflow due to water recharge into pre-formed bed separation.

Before the abnormal water inrush events occurred at the panel on 2 May, 17 June, and 14 July 2014, the mining height of the coal seam remained relatively large for several consecutive days, indicating that the water inflow rate of the panel was positively correlated with the mining height (Figure 10). During two periods with similar mining distances: 20–25 June and 18 July–2 August, multiple abnormal water inrush events occurred at the panel. Correspondingly, the water level of the Luohe Formation declined during these periods (Figure 11), indicating the occurrence of re-inflow due to water recharge into pre-formed bed separation. When abnormal water inrush occurred on 17, 20, 22, and 25 June 2014, the water level of the Luohe Formation exhibited a zigzag variation trend: the water level rose continuously before water inrush and dropped sharply after water inrush. This indicates that the abnormal water inrush events from 17 to 25 June were dominated by water inrush from the bed separation and re-inflow due to water recharge into pre-formed bed separation. During several abnormal water inrush events after 14 July, compared with the water level after the previous water inrush, the water level of the Luohe Formation not only exhibited an obvious zigzag trend but also remained stable in some cases.

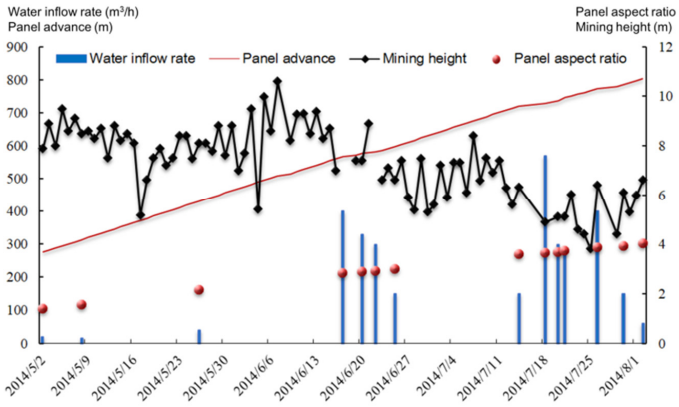


Figure 10. Water inrush curve and mining height during advancement of 21303 panel.

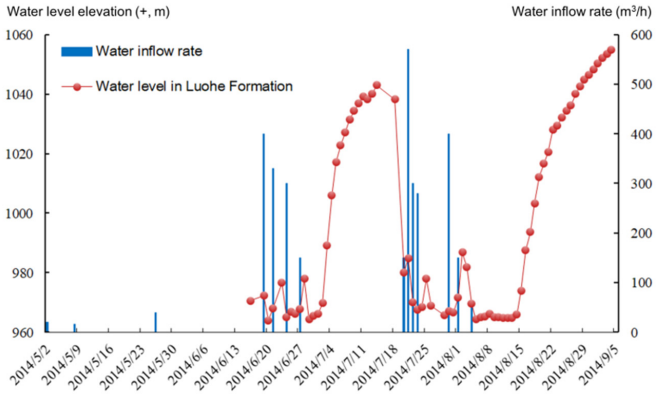


Figure 11. Groundwater variation curve in the Luohe Formation during advancement of 21303 panel.

The detection results of geophysical anomalies indicate that low-resistivity anomalies at 60 m and 90 m above the coal seam almost cover the entire panel, suggesting a certain correlation between the abnormal water inflow in the panel and the water-rich anomalies in the overburden of the coal seam roof (Figure 12). The Luohe Formation sandstone aquifer above the coal seam serves as the primary water source for bed separation water accumulation.

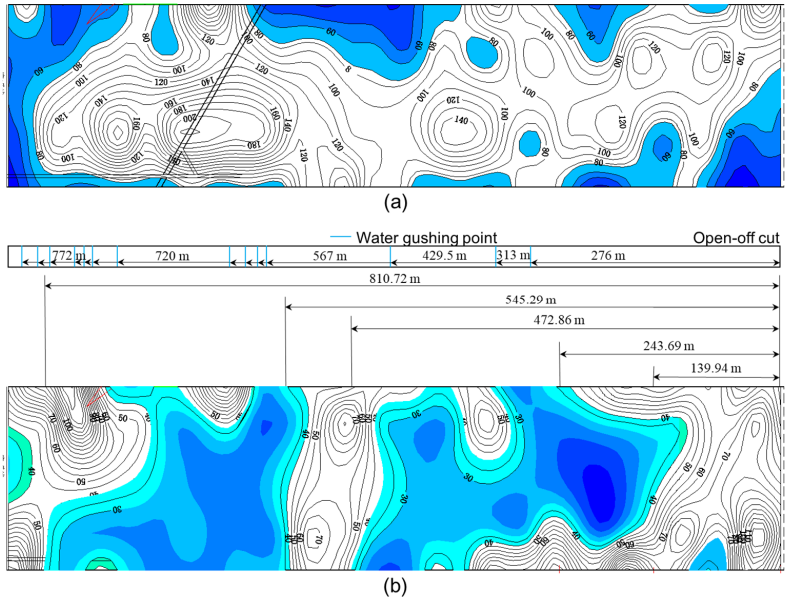


Figure 12. Transient electromagnetic survey results of panel 21303: (**a**) 90 m above the coal seam roof, (**b**) 60 m above the coal seam roof.

4.3.2. Hazard Prevention Model of Bed Separation Water Inrush Based on FAHP

The hazard of bed separation water inrush occurs when the overburden simultaneously satisfies three conditions: the existence of a water-accumulating bed separation, a water recharge source, and a water-conducting channel. The development of water-accumulating bed separation and water-conducting channels is affected by multiple factors, including the thickness of aquifers and aquicludes, mining conditions, panel parameters, and hydrostatic pressure, collectively leading to the hazards of bed separation water inrush with different risk levels.

A Fuzzy Analytic Hierarchy Process (FAHP) hierarchical model is developed, with hazard identification and prevention measures for bed separation water hazards serving as the criteria layer for hazard prevention. The indicator-layer factors are determined according to the criteria-layer indicators, followed by a comprehensive analysis of all factors in the indicator layer. In accordance with the principle that lower-level elements are directly controlled by the next higher level and the membership relationships between indicators, a primary indicator layer and a secondary indicator layer are established (Figure 13). An Experts Grading System (EGS) is adopted to compare the importance of indicator factors at the same hierarchical level and assign corresponding scores, and a fuzzy consistent judgment matrix is constructed (Table 3). According to the complementarity principle and fuzzy consistency principle of the fuzzy matrix F_{ij}, $F_{ij} = (f_{ij})_{nn}$ is a fuzzy consistent complementary matrix that satisfies: $f_{ij} + f_{ji} = 1, f_{ij} = f_{ik} - f_{jk} + 0.5$ $(i, j, k \in Q)$.

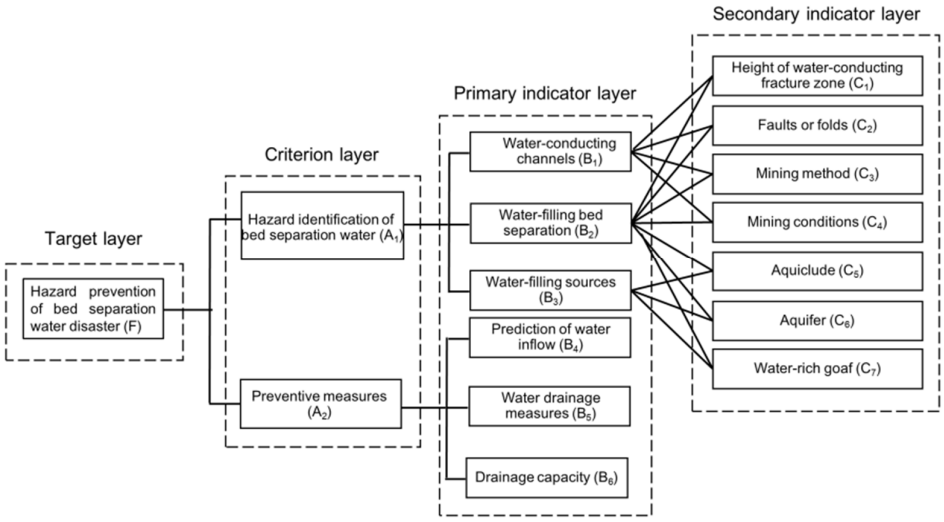


Figure 13. FAHP hierarchical model.

Table 3. Value standard assignment of indicator importance.

Importance Weight Assignment	Explanation of Importance Level Assignment
$0.1 \leq f_{ij} < 0.5$	Compared with factor f_i, factor f_j is more important; the smaller f_{ij} is, the higher the importance of f_j.
$f_{ij} = 0.5$	Factor f_i is as important as factor f_j.
$0.5 < f_{ij} \leq 0.9$	Compared with factor f_j, factor f_i is more important, and the larger f_{ij} is, the higher the importance of f_i.

According to the membership relationships at different levels, the weights of the indicators at the same hierarchical level are calculated respectively, that is

$$\omega_i = \frac{1}{n} - \frac{1}{2a} + \frac{1}{an}\sum_{k=1}^{n} f_{ik}, \tag{5}$$

where a is the non-negative constant, $a = \frac{n-1}{2}$.

The relative weights are calculated based on the membership degree of the first-order hierarchy corresponding to a specific index in the higher-order hierarchy. Finally, the comprehensive weights of each indicator in the lowest-level indicator layer with respect to the overall objective (F) are determined according to the membership relationships among different hierarchies. Assuming that the weight of the i-th indicator in the criteria layer (A) relative to the overall objective (F) is denoted as ω_i, then the weight vector matrix of the criteria layer is represented as

$$\omega_{F-A} = \left\{\omega_1^A, \quad \omega_2^A, \quad \cdots, \quad \omega_n^A\right\}, \tag{6}$$

The weight vector matrix of each indicator in the indicator layer (B) corresponding to each indicator in the criteria layer (A) is

$$\omega_{A-B} = \left\{\omega_1^B, \quad \omega_2^B, \quad \cdots, \quad \omega_n^B\right\}, \tag{7}$$

Then the comprehensive weights of each indicator in the indicator layer (B) with respect to the overall objective (F) are

$$\omega_{F-B} = \omega_{F-A} \times \omega_{A-B}, \tag{8}$$

According to the FAHP hierarchical model, complementary matrices are established for the criteria layer and indicator layer, respectively. The prevention of hazards caused by bed separation water hazards is divided into a three-level hierarchical model. The corresponding hierarchical model is constructed based on the principle of fuzzy consistent complementary matrices (Table 4). By substituting these into Equation (5), the weights of different levels are calculated as follows:

F-A judgment matrix: $\omega(A_1) = 0.5$, $\omega(A_2) = 0.5$,
A_1-*B* judgment matrix: $\omega(B_1) = 0.3333$, $\omega(B_2) = 0.3333$, $\omega(B_3) = 0.3333$,
A_2-*B* judgment matrix: $\omega(B_4) = 0.3$, $\omega(B_5) = 0.2$, $\omega(B_6) = 0.5$,
B-A judgment matrix: $\omega(C_1) = 0.2238$, $\omega(C_2) = 0.1238$, $\omega(C_3) = 0.1571$, $\omega(C_4) = 0.1571$, $\omega(C_5) = 0.0857$, $\omega(C_6) = 0.1619$, $\omega(C_7) = 0.0905$

According to Equations (6)–(8), the comprehensive weights of each indicator in the indicator layer with respect to the objective layer are obtained (Table 5). The importance ranking of bed separation water hazard prevention indicators shows that drainage capacity, predicted water inflow, development height of the water-conducting fractured zone, and water drainage and release measures are the four most significant indicators. Analysis of the bed separation water hazard prevention model using the Fuzzy Analytic Hierarchy Process (FAHP) indicates that increasing drainage capacity and accurately predicting water inflow from bed separation are two effective measures to prevent the occurrence of bed separation water hazards or reduce the hazard risk index. In addition, controlling the development of the water-conducting fractured zone and optimizing water drainage and release measures are also effective approaches to reduce the risk coefficient of hazards induced by bed separation water.

Table 4. Judgment matrix. (**a**) *F-A* judgment matrix. (**b**) A_1-*B* judgment matrix. (**c**) A_2-*B* judgment matrix. (**d**) *B-C* judgment matrix.

(**a**)		
F-A	A_1	A_2
A_1	0.5	0.5
A_2	0.5	0.5

(**b**)			
A_1***-B***	B_1	B_2	B_3
B_1	0.5	0.5	0.5
B_2	0.5	0.5	0.5
B_3	0.5	0.5	0.5

(**c**)			
A_2***-B***	B_4	B_5	B_6
B_4	0.5	0.6	0.3
B_5	0.4	0.5	0.2
B_6	0.7	0.8	0.5

(**d**)							
B-C	C_1	C_2	C_3	C_4	C_5	C_6	C_7
C_1	0.5	0.8	0.7	0.7	0.9	0.7	0.9
C_2	0.2	0.5	0.4	0.4	0.6	0.4	0.6
C_3	0.3	0.6	0.5	0.5	0.7	0.5	0.7
C_4	0.3	0.6	0.5	0.5	0.7	0.5	0.7
C_5	0.1	0.4	0.3	0.3	0.5	0.2	0.5
C_6	0.3	0.6	0.5	0.5	0.8	0.5	0.7
C_7	0.1	0.4	0.3	0.3	0.5	0.3	0.5

Table 5. The total hierarchical order and comprehensive weight.

Indicator				***A1***	***A2***	**Comprehensive Weight**	**Importance Ranking**
				0.5	**0.5**		
C1	0.2238					0.1119	3
C2	0.1238	***B1***	0.3333			0.0619	8
C3	0.1571					0.0785	6
C4	0.1571	***B2***	0.3333			0.0785	6
C5	0.0857					0.0429	10
C6	0.1619	***B3***	0.3333			0.0810	5
C7	0.0905					0.0453	9
		B4	0.3			0.1500	2
		B5	0.2			0.1000	4
		B6	0.5			0.2500	1

5. Conclusions

This study investigates the disaster-causing factors of bed separation water hazards, the prediction of water-filled bed separation, and the prevention and control of such hazards, thus revealing the water inrush mechanism of bed separation water hazards. The study innovatively proposes the volume expansion mechanism of water-filled bed separation and the prevention and control technology for bed separation water inrush hazards, which are verified by numerical simulation and field measurement. This case study involves the Cui'mu Coal Mine in Shaanxi Province of China.

The results of numerical simulation, theoretical calculation and field measurement are in good agreement. Water accumulation within the bed separation can increase the volume of the bed separation. The occurrence of bed separation water hazards is mainly caused by the water-conducting fractured zone induced by mining disturbance penetrating the water-filled bed separation. Field test results demonstrate that the height of the water-conducting fractured zone is positively correlated with the mining height of the coal seam. Numerical simulation results indicate that water accumulation in the bed separation increases the deformation of the overburden under the bed separation and expands the volume of the bed separation to a certain extent. Moreover, the deformation of the overburden increases progressively with rising hydrostatic pressure.

This study predicts the enhancing effect of water accumulation in bed separation on both the expansion of the bed separation and water inrush volume, which is verified through theoretical calculation, numerical simulation, and field measurement. A bed separation water hazard exists when three conditions are simultaneously present: the development of water-filled bed separation in the overburden, a water source for filling the bed separation, and a water-conducting channel from the panel to the water-filled bed separation. The formation of water-filled bed separation and water-conducting channels is influenced by multiple factors, including the thickness of aquifers and aquicludes, mining conditions, panel conditions, and hydrostatic pressure, leading to bed separation water hazards of varying risk levels. The Fuzzy Analytic Hierarchy Process (FAHP) is an effective method for reducing the occurrence of such hazards by assessing the likelihood of bed separation water formation and by enabling proactive drainage. Furthermore, this case provides a practical example for analyzing and controlling bed separation water hazards. Therefore, bed separation water hazards can be effectively prevented and controlled through accurate prediction and advanced drainage.

Funding: The author declares that financial support was received for the research and/or publication of this article. This study was supported by the General Project of Shaanxi Provincial Natural Science Foundation of China (No. 2024JC-YBQN-0335), and the Anhui Provincial Fund for Postdoctoral Researchers' Scientific Research (No. 2023B749).

Data Availability Statement: The original contributions presented in this study are included in the article. Further inquiries can be directed to the corresponding author.

Acknowledgments: The authors would like to acknowledge the anonymous reviewers for their detailed comments that helped to improve this study. The authors are grateful to Yajun Sun from China University of Mining and Technology for reviewing the manuscript and providing valuable suggestions, as well as to Wanghua Sui from the same institution for his guidance on the experiments.

Conflicts of Interest: Author Hewen Ma was employed by the company CCTEG Xi'an Research Institute (Group) Co., Ltd. and Huaibei Mining Group Co., Ltd. The author declares that the research was conducted in the absence of any commercial or financial relationships that could be construed as a potential conflict of interest.

References

1. Xu, Z.; Sun, Y.; Gao, S.; Zhao, X.; Duan, R.; Yao, M.; Liu, Q. Groundwater source discrimination and proportion determination of mine inflow using ion analyses: A case study from the Longmen Coal Mine, Henan Province, China. *Mine Water Environ.* **2018**, *37*, 385–392. [CrossRef]
2. Chen, S.; Yin, D.; Gao, F.; Liu, Y.; Ren, K. An overview of integrated surface subsidence-reducing technology in mining areas of China. *Nat. Hazards* **2016**, *81*, 1129–1145. [CrossRef]
3. Xuan, D.; Xu, J. Longwall surface subsidence control by technology of isolated overburden grout injection. *Int. J. Min. Sci. Technol.* **2017**, *27*, 813–818. [CrossRef]
4. Zhu, X.; Guo, G.; Liu, H.; Yang, X. Surface subsidence prediction method of backfill-strip mining in coal mining. *Bull. Eng. Geol. Environ.* **2019**, *78*, 6235–6248. [CrossRef]

5. Wang, R.; Bai, J.; Yan, S.; Chang, Z.; Wang, X. An innovative approach to theoretical analysis of partitioned width & stability of strip pillar in strip mining. *Int. J. Rock Mech. Min. Sci.* **2020**, *129*, 104301.
6. Chen, G.; Xu, Z.; Sun, Y.; Sui, W.; Li, X.; Zhao, X.; Liu, Q. Minewater deep transfer and storage. *J. Clean. Prod.* **2022**, *332*, 129848. [CrossRef]
7. Hu, Y.; Li, W.; Wang, Q.; Liu, S.; Wang, Z. Evolution of floor water inrush from a structural fractured zone with Confined Water. *Mine Water Environ.* **2019**, *38*, 252–260. [CrossRef]
8. Wang, Z.; Li, W.; Hu, Y. Experimental study on mechanical behavior, permeability, and damage characteristics of Jurassic sandstone under varying stress paths. *Bull. Eng. Geol. Environ.* **2021**, *80*, 4423–4439. [CrossRef]
9. Ma, H. Characteristics analysis of bed separation water inrush hazard of coal mine areas in China. *Saf. Coal Mines* **2023**, *54*, 106–112.
10. Dong, S.; Wang, H.; Guo, X.; Zhou, Z. Characteristics of water hazards in China's coal mines: A review. *Mine Water Environ.* **2021**, *40*, 325–333. [CrossRef]
11. Gui, H.; Tong, S.; Qiu, W.; Lin, M. Research on preventive technologies for bed-separation water hazard in China coal mines. *Appl. Water Sci.* **2018**, *8*, 7. [CrossRef]
12. Chen, W.; Li, W.; He, J.; Qiao, W.; Wang, Q.; Yang, Y. Impact of mining-induced bed separation spaces on a cretaceous aquifer: A case study of the Yingpanhao coal mine, Ordos Basin, China. *Hydrogeol. J.* **2022**, *30*, 691–706. [CrossRef]
13. Qiao, W.; Li, W.; Li, X. Mechanism of "hydrostatic water-inrush" and countermeasures for water inrush in roof bed separation of a mining face. *J. Min. Saf. Eng.* **2011**, *28*, 96–103.
14. Qiao, W.; Wang, Z.; Li, W.; Lu, Y.; Li, L.; Huang, Y.; He, J.; Li, X.; Zhao, S.; Liu, M. Formation mechanism, disaster-causing mechanism and prevention technology of roof bed separation water disaster in coal mines. *J. China Coal Soc.* **2021**, *46*, 507–522.
15. Fan, K.; Li, W.; Wang, Q.; Liu, S.; Xue, S.; Xie, C.; Wang, Z. Formation mechanism and prediction method of water inrush from separated layers within coal seam mining: A case study in the Shilawusu mining area, China. *Eng. Fail. Anal.* **2019**, *103*, 158–172. [CrossRef]
16. Wu, L.; Bai, H.; Ma, D. Prediction and prevention of water inrush hazards from bed separation space. *Mine Water Environ.* **2021**, *40*, 657–670. [CrossRef]
17. Wang, F.; Xu, J.; Chen, S.; Ren, M. Method to predict the height of the water conducting fractured zone based on bearing structures in the overlying Strata. *Mine Water Environ.* **2019**, *38*, 767–779. [CrossRef]
18. Ou, Q.; Chen, L.; Hou, X.; Fan, L.; Chen, Y.; He, D.; Song, J. Identification and evaluation of bed separation induced by mining based on beam-column and stress-balanced arch theory. *Eng. Fail. Anal.* **2024**, *157*, 107961. [CrossRef]
19. Ma, H.; Sui, W.; Ni, J. Environmentally sustainable mining: A case study on surface subsidence control of grouting into overburden. *Environ. Earth Sci.* **2019**, *78*, 320. [CrossRef]
20. Liang, S.; Zhang, X.; Ke, F.; Liu, J.; Yao, Q.; Luo, H.; Li, X.; Xu, Y. Evolution of overlying strata bed separation and water inrush hazard assessment in fully mechanized longwall top-coal caving of an ultra-thick coal seam. *Water* **2025**, *17*, 850. [CrossRef]
21. Xuan, D.; Xu, J.; Zhu, W. Dynamic disaster control under a massive igneous sill by grouting from surface boreholes. *Int. J. Rock Mech. Min. Sci.* **2014**, *71*, 176–187. [CrossRef]
22. Fan, K.; Li, W.; Wang, Q.; Chen, W.; Yang, Y. Distribution characteristic of mining-induced horizontal fracture in longwall panel: Field investigation and prediction model. *Eng. Fail. Anal.* **2022**, *142*, 106778. [CrossRef]
23. Xuan, D.; Xu, J. Grout injection into bed separation to control surface subsidence during longwall mining under villages: Case study of Liudian coal mine, China. *Nat. Hazards* **2014**, *73*, 883–906. [CrossRef]
24. Ma, H.; Ji, Y.; Wang, S. Calculation of subsidence due to longwall mining with overburden grouting and its application. *Geofluids* **2022**, *2022*, 2357060. [CrossRef]
25. Jiránková, E.; Petroš, V.; Šancer, J. The Assessment of stress in an exploited rock mass based on the disturbance of the rigid overlying strata. *Int. J. Rock Mech. Min. Sci.* **2012**, *50*, 77–82. [CrossRef]
26. Xuan, D.; Xu, J.; Wang, B.; Teng, H. Borehole investigation of the effectiveness of grout injection technology on coal mine subsidence control. *Rock Mech. Rock Eng.* **2015**, *48*, 2435–2445. [CrossRef]
27. Peng, S.S. *Coal Mine Ground Control*, 2nd ed.; John Wiley & Sons: New York, NY, USA, 1986.
28. *GB 50021-2001*; Code for Investigation of Geotechnical Engineering. China Architecture & Building Press: Beijing, China, 2002.
29. Hu, B.; Zhang, H.; Shen, B. *State Administration of Work Safety (2017) Regulations for Setting Pillar and Mining Under Buildings, Railways and Water Bodies*; Coal Industry Press: Beijing, China, 2017.

Disclaimer/Publisher's Note: The statements, opinions and data contained in all publications are solely those of the individual author(s) and contributor(s) and not of MDPI and/or the editor(s). MDPI and/or the editor(s) disclaim responsibility for any injury to people or property resulting from any ideas, methods, instructions or products referred to in the content.